Spatial Distance Effect of Bienzymes on the Efficiency of Sequential Reactions in a Microfluidic Reactor Packed with Enzyme-immobilized Microbeads

Jinseok HEO

Department of Chemistry, The State University of New York College at Buffalo, 1300 Elmwood Ave., Buffalo, NY 14222, USA

Three different configurations of microfluidic reactors packed with enzyme-bearing microbeads were examined to show that the overall efficiency of coupled enzyme-catalyzed reactions depends on the spatial relationship of two enzymes immobilized on the bead surfaces. The spatial distances of glucose oxidase (GOx) and horseradish peroxidase (HRP) enzymes were controlled by using microbeads as a supporting matrix for immobilizing the two enzymes and packing them in two microfluidic chambers. A microreactor packed with microbeads coimmobilized with the two enzymes showed a better overall reaction efficiency than the other two reactors, where the two enzymes were spatially distant, under a flow condition. These results are ascribed to the reduced diffusional loss of an intermediate product in the bienzyme-coimmobilized microreactor. Furthermore, the inhibition of the GOx enzyme by H_2O_2, an intermediate product, can be eliminated by quickly converting H_2O_2 to a final non-inhibiting product in the bienzyme-coimmobilized microreactor.

**Keywords** Microfluidic reactor, sequential enzyme reaction, enzyme immobilization

Introduction

Here, we present three different configurations of microfluidic reactors that carry out sequential, two-step, enzyme-catalyzed reactions under flow conditions (Scheme 1). In all of these configurations, substrate molecules are delivered to the reactor zone by a pressure-driven flow, encountered by the bead-immobilized enzymes, and converted into products. We find that the overall rate of product generation depends on the spatial relationship of the two enzymes. In reactor **I**, both enzymes were co-immobilized on a single set of beads. In reactor **II**, the enzyme required to catalyze the first step of the reaction sequence was immobilized on one set of beads, and the enzyme necessary to catalyze the second step was immobilized on a second set of beads. The two-step reaction was then carried out by sequentially passing the substrate over the two sets of beads. In reactor **III**, the two sets of enzyme-immobilized beads were mixed. Experiments showed that the reactor **I** configuration resulted in a more effective substrate turnover. Our results clearly demonstrate the usefulness of a microfabricated system and enzyme-immobilized beads in designing an efficient, multi-step microfluidic reactor based on immobilized enzymes.

Immobilized-enzymes have been widely used in various areas, including the food industry, pharmaceutical medicine, biomedical engineering, biofuel production, and environmental remediation because of the convenient recovery process of

enzymes from solution and the potential reuse of the enzymes.[1] Recently, microfabrication technology has opened up a new era in the applications of immobilized enzymes.[2,3] Microfluidic reactors based on immobilized enzymes have been broadly applied for proteomics,[4] drug discovery,[5-7] small scale synthesis of compounds,[8-12] kinetic study of immobilized enzymes,[13-15] and biosensing.[16-18] Microfluidic reactors have been an attractive
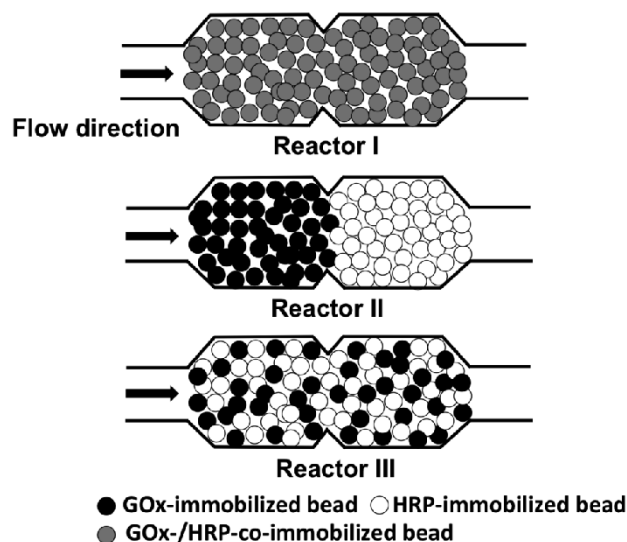
Scheme 1   Three different configurations of microfluidic reactors.

To whom correspondence should be addressed.
E-mail: heoj@buffalostate.edu

platform for these applications, because they consume small amounts of reagents, and their dimensions are small enough to handle or mimic a biological system at a cellular level.

While many of the previous applications rely on a single-step enzyme reaction, the applications of multiple immobilized enzymes in the microfluidic reactor to perform multi-step, consecutive reactions have been growing.[11,18-22] This is partly because there are increasing interests in using multiple enzymes for synthesizing new compounds and in developing synthetic biology. It has been previously reported that multiple enzymes can be either co-immobilized on a surface[19,20] or within a matrix[18] in proximity, or be immobilized separately[11,19,21,22] on discrete zones of a microreactor, which are assigned for each of the enzymes. Intuitively, it is expected that the spatial distances between the multiple enzymes will affect the overall efficiency of the coupled enzyme reactions. In the early 1970's Mosbach noted the importance of the spatial relationship of bienzymes on the overall reaction efficiency.[23,24] However, their study was performed using a large scale of enzyme-immobilized polymeric matrices under a non-fluidic condition. Therefore, it is difficult to adopt their results in a small-scale reaction system under a fluidic condition, at which we are aiming.

Our report demonstrates the relative effectiveness of different catalyst configurations for carrying out sequential reactions within microfluidic systems. Here, polymeric microbeads were selected as a supporting matrix for immobilizing two different enzymes. These microbeads can provide a large surface-to-volume ratio for immobilizing enzymes, efficiently mix laminar flows, and reduce the diffusional distances of substrate molecules to the enzymes on the bead surfaces. More importantly, they can be conveniently used to control the spatial distances of multiple enzymes, as demonstrated in this report. The sequential enzymatic reactions shown in Scheme 2 were used to examine the effect of spatial distances of the two enzymes on the substrate turnover. The experimental results showed that the overall reaction efficiency of the reactor **I** in Scheme 1 was much higher than the other two reactors (**II** and **III** in Scheme 1). This report will discuss the results in terms of two effects: the molecular mass transport of an intermediate product and the inhibition of glucose oxidase (GOx) enzyme by the intermediate product generated during the sequential enzyme reactions.

Experimental

Reagents and chemicals

Poly(dimethylsiloxane) (PDMS) prepolymer (Sylgard 184) was purchased from Dow Corning Co. (Midland, MI). Positive photoresist (AZ P4620) and developer solution (AZ 421K) were purchased from AZ Electronic Materials. (Branchburg, NJ). Biotin amidocaproyl-labeled glucose oxidase (biotin-GOx, M_W = 160 kDa, from *Aspergillus niger*), biotin amidocaproyl-labeled peroxidase (biotin-HRP, type VI, M_W = 44 kDa, from *Horseradish*), horseradish peroxidase (HRP, type VI-A, from *Horseradish*), glucose, biotin-fluorescein, H_2O_2 (analytical reagent, 30 wt%), and resorufin were purchased from Sigma Chemical Co. (St. Louis, MO). Avidin-coated microbeads (SuperAvidin™ Coated Microspheres, 9.95 μm diameter) were obtained from Bangs Laboratories, Inc. (Fishers, IN). Phosphate buffered saline (PBS) solution was prepared by dissolving 130 mmol of NaCl, 2.7 mmol of KCl, 10 mmol of Na_2HPO_4 (Sigma) and 1.8 mmol of KH_2PO_4 (Sigma) in 1 L of deionized water and adjusting the pH to 7.4 with HCl or NaOH. Similarly, 50 mM Tris buffer solution was prepared by dissolving
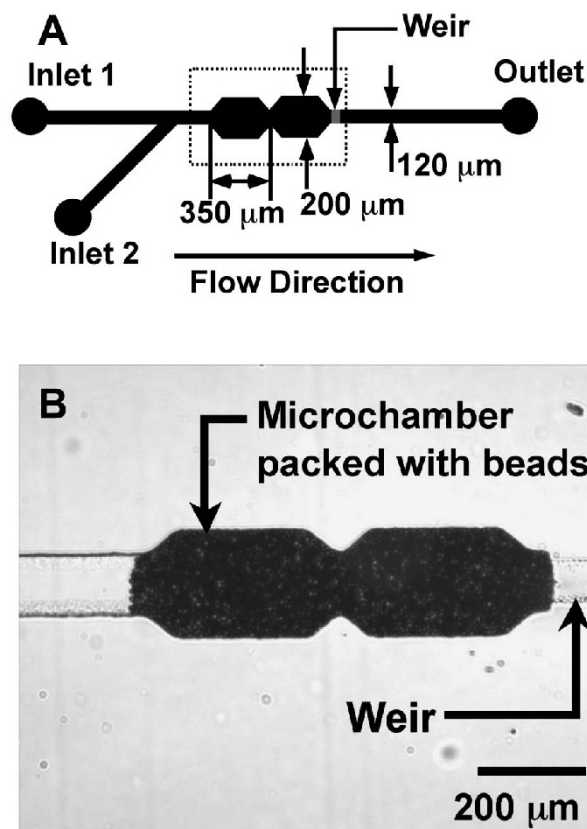

Fig. 1 (A) Schematic diagram of a microfluidic reactor used for tests. (B) Optical micrograph showing the region of the device enclosed within the black dotted box in Fig. 1(A).

41.4 mmol of tris(hydroxymethyl)aminomethane hydrochloride (Sigma) and 8.6 mmol of the base form in 1 L of deionized water and adjusting the pH to 7.4 with HCl or NaOH. Amplex Red (*N*-acetyl-3,7-dihydroxyphenoxazin-3-one) was purchased from Invitrogen, Inc. (Eugene, OR). All aqueous solutions were prepared using 18 MΩ-cm water.

Preparation of microfluidic reactors packed with enzyme-immobilized beads

The microfluidic bioreactors used in this study were fabricated using a previously reported procedure (see the procedures in Supporting Information).[22] A schematic illustration of the device design is shown in Fig. 1A. Three different sets of enzyme-bearing beads (HRP-bearing beads, GOx-bearing beads, and GOx-/HRP-bearing beads) were prepared using biotinylated enzymes and avidin-coated microbeads (see the procedures in Supporting Information). The beads co-immobilized with the GOx and HRP enzymes had a roughly the same mole numbers of GOx and HRP enzymes on their surfaces.

Enzyme-modified microbeads (3.66×10^5 beads/mL in buffer) were introduced to the microreactor *via* inlet 2 (Fig. 1A) using a syringe. PBS buffer was simultaneously injected into inlet 1 to control the rate of bead deposition in the microchambers. Reactor **I** (Scheme 1) was prepared by introducing microbeads co-conjugated with both GOx and HRP into both microchambers. Reactor **II** was prepared by first introducing HRP-conjugated microbeads into the chamber on the right side of the device and then GOx-conjugated microbeads were introduced into the chamber on the left. Reactor **III** was prepared by introducing a bead solution, which was prepared by mixing GOx-conjugated
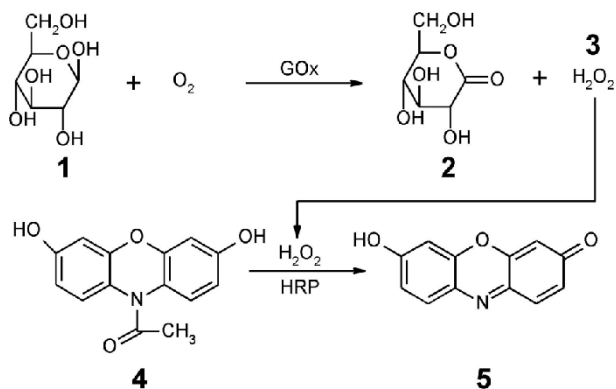
Scheme 2 Two-step, sequential enzyme reactions employed in microfluidic reactors.

and HRP-conjugated microbeads in a 1:1 volume ratio, into all microchambers.

Test of microfluidic reactors

A 0.500 M glucose stock solution was prepared in Tris buffer (pH 7.4) and stored at room temperature for one day prior to use. The stock solution was diluted with Tris buffer to prepare lower concentrations. Amplex Red solutions (40 mM) were prepared in anhydrous DMSO and stored in 20 μL aliquots at –20°C until just before use. A solution containing 1.00 mM glucose and 0.80 mM Amplex Red in Tris buffer (pH 7.4) was pumped through inlet 1 at a flow rate of 0.5 μL/min using a syringe pump (PHD 2000, Harvard Apparatus, Hollistion, MA) until the solution emerged from inlet 2 (Fig. 1A). Next, the opening of inlet 2 was plugged with a Teflon stopper, and then the glucose test solution was introduced into inlet 1 at a flow rate of 0.20, 0,15, 0.10 and, 0.05 μL/min, respectively. The fluorescent product (resorufin) of the coupled reactions (**5** in Scheme 2) was observed 0.17 mm downstream of the end of the microreactor using an epifluorescence microscope (Nikon Eclipse TE 300, Nikon Co., Tokyo, Japan) equipped with a mercury lamp and a cube-type band-pass filter (XF-102-2 filter set, Omega Optical, Inc., Brattleboro, VT). Using a 16-bit gray-scale CCD camera (Photometrics Ltd., Tucson, AZ), fluorescence micrographs were acquired every 30 s for up to 20 min until a steady state fluorescence signal was reached. The integration time for all fluorescence micrographs was 0.7 s, and the microdevices were only illuminated during data acquisition to minimize photobleaching. The test outlined above was repeated two more times using independently prepared microfluidic reactors.

Results and Discussion

Preparation of microfluidic reactors packed with enzyme-immobilized beads

Figure 1A is a schematic illustration of the microfluidic device used in these experiments, and Fig. 1B is an optical micrograph showing the region of the device enclosed within the dotted lines in Fig. 1A. The microchambers and channels were ~22 μm high, which was measured from the photoresist master using a profilometer; the remaining dimensions are provided in Fig. 1A. The volume of each of the two microchambers was ~1.5 nL. The gap between the top of the weir structure (Fig. 1B) and the floor of the channel was 6 μm, so it was able to retain

the 10 μm-diameter beads used to immobilize the enzymes. The microbeads were packed into the microchambers using a syringe. The void fraction of a bead-packed microchamber of the sort used here has been estimated to be 0.5.[15,25] This is reasonable, considering that the packing fraction of perfect hexagonal close packing is 0.74. Taking the void fraction into account, the estimated number of microbeads packed in each microchamber is 1350.

The maximum binding capacities of avidin-coated beads for biotin–GOx and biotin–HRP enzymes were measured independently (Fig. S1, Supporting Information). Only ~50% of the biotin-binding sites on the avidin-coated beads were available for each of the enzymes. These results suggest that by considering the protein foot areas of GOx (50 nm^2)[26] and HRP (20 nm^2)[27] to be comparable to that of avidin (34 nm^2),[21] only one out of two biotin-binding sites of an avidin molecule (note that we assumed only two biotin-binding sites are present for one avidin molecule sitting on a bead surface, because two other binding sites are oriented toward the bead surface) is available for a biotin–GOx or biotin–HRP enzyme molecule. Thus, only one molecule of biotin–GOx or biotin–HRP can be bound to one avidin molecule.

After this confirmation, the GOx-bearing beads and the HRP-bearing beads, which were fully covered by the GOx and HRP enzymes, respectively, were prepared by incubating the avidin beads with sufficient amounts of biotin–GOx and biotin–HRP, respectively. The surface concentrations of GOx and HRP enzymes prepared on each set of microbeads are approximately the same if the avidin sites of bead surfaces are saturated with the enzymes, because the avidin molecule on a bead surface cannot accommodate more than one molecule of biotin–GOx or biotin–HRP. The beads co-immobilized with biotin–GOx and biotin–HRP were prepared by incubating the avidin beads with a solution consisting of biotin–GOx and biotin–HRP enzymes in one-to-one mole ratio. The total mole numbers of biotinylated enzymes added were sufficient to fully cover the avidin molecules on the beads. In this manner the avidin molecules could be covered with equal mole numbers of biotin–GOx and biotin–HRP enzymes. It is expected that the affinities of biotin–GOx and biotin–HRP are similar to each other, because a spacer group (C11) is present between the biotin and the enzymes, and so the affinity of biotinylated enzymes to avidin is less likely to be affected by the enzymes.

A potential problem of steric hindrance between GOx and HRP enzymes on a bead surface was examined. Only ~62% of the surface area of each bead is occupied with avidin, which is estimated from the surface area and concentration of avidin (34 nm^2 and 5.72 × 10^6 molecules/bead). If half of the avidin molecules are occupied by biotin–GOx and the other half by biotin–HRP, then the two enzymes cover ~64% of the bead surface. This means that even at maximum coverage there is substantial free area remaining on the bead surface, and therefore the enzymes are not likely to sterically interfere with one another. This conclusion was supported by our observation that the order of immobilization for the beads supporting both enzymes (first GOx and then HRP, first HRP and then GOx, or simultaneous co-immobilization of both) did not affect their activity (Fig. S2, Supporting Information).

It has previously been reported that PDMS channels having aspect ratios (width/height) of ~80 are subject to bulging, and that this effect can bias fluorescence measurements obtained at different flow rates.[28] However, no change in fluorescence was observed at a flow rate of up to 1.00 μL/min in a microfluidic reactor packed with microbeads (Fig. S3, Supporting Information). This is because we fabricated a microfluidic
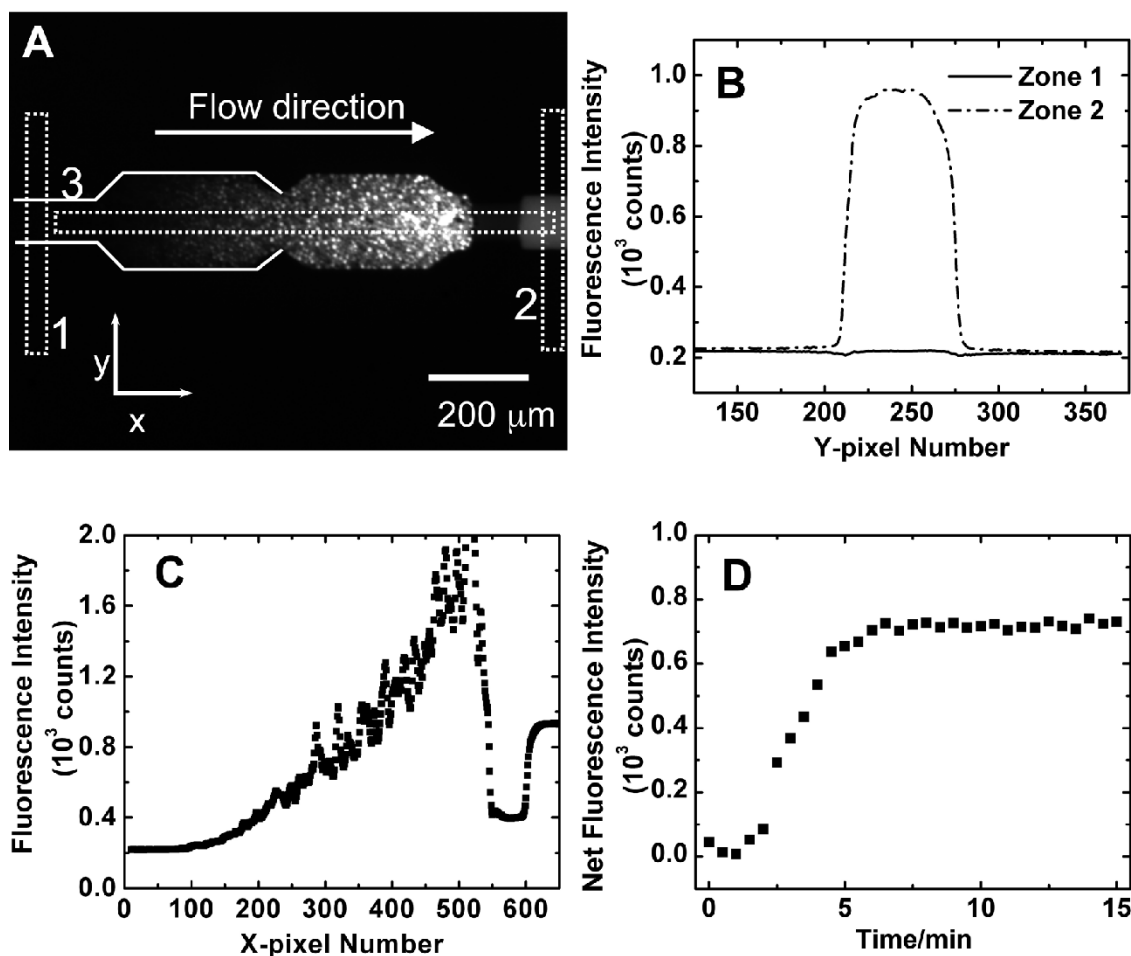
Fig. 2   (A) Fluorescence micrograph of reactor **I** obtained 15 min after a reactant solution consisting of 1.00 mM glucose and 0.80 mM Amplex Red was introduced into the reactor at a flow rate of 0.20 μL/min. The microbeads were co-immobilized with GOx and HRP enzymes. (B) Fluorescence intensity profiles obtained from zones 1 and 2 indicated by the white dotted boxes shown in Fig. 2(A). (C) Fluorescence intensity profile obtained from zone 3 indicated by the white dotted box shown in Fig. 2(A). (D) Plot of time-dependent net fluorescence intensity. The net fluorescence intensity was obtained by subtracting the average intensity of zone 1 from that of zone 2 in the channel shown in Fig. 2(A). The x and y pixel dimensions are 2 μm, respectively.

reactor having a low aspect ratio ranging from 5 – 9. Accordingly, flow rates in the range of 0.05 to 0.20 μL/min were used for the experiments reported here.

Test of the microreactors

Products of coupled reactions shown in Scheme 2 were examined as a function of the location of the two enzymes within the microreactors. This amounts to introducing glucose (**1**) and Amplex Red (**4**) into the microreactor, and then measuring the fluorescence arising from the product (resorufin, **5**) of the coupled enzyme-catalyzed reactions. The experiment was set up by introducing a 50 mM Tris buffer solution (pH 7.4) containing 1.00 mM glucose and 0.80 mM Amplex Red into the microreactor at a flow rate of 0.20 μL/min. Fluorescence micrographs were collected every 30 s for 20 min. Figure 2A shows a typical fluorescence micrograph obtained at 15 min after the reactant solution was continuously pumped into the channel of reactor **I**. The fluorescence-intensity profiles shown in Fig. 2B were obtained from the two zones of the microreactor enclosed within the white dotted boxes 1 and 2 in Fig. 2A. The stronger signal at zone 2 compared with zone 1 indicates the generation of a fluorescence product after the two-step sequential reactions. Figure 2C shows the fluorescence intensity profile obtained from the region of the microreactor enclosed within the white dotted box 3 in Fig. 2A. This intensity profile clearly shows an increase of fluorescence intensity along the flow direction, suggesting the accumulation of product from the bead bed along the flow direction in the microfluidic reactor. The fluorescence intensity measured from region 2 (x-pixel number: >600) was 4-times that measured from the region of the weir structure (x-pixel number: 550 – 600). This fluorescence-intensity ratio reflects the height difference between the detection region (22 μm) and the weir region (6 μm). Figure 2D shows a graph of the time-dependent net fluorescence intensity extracted from fluorescence micrographs similar to Fig. 2A. The net fluorescence intensity was obtained by subtracting the average fluorescence intensity of zone 1 from that of zone 2. Because the net fluorescence intensity reached a steady state within 10 min after the introduction of reactants, the data points between 10 and 15 min were averaged to obtain the average value of the net fluorescence intensity. A steady state fluorescence intensity can be achieved when the mass transport
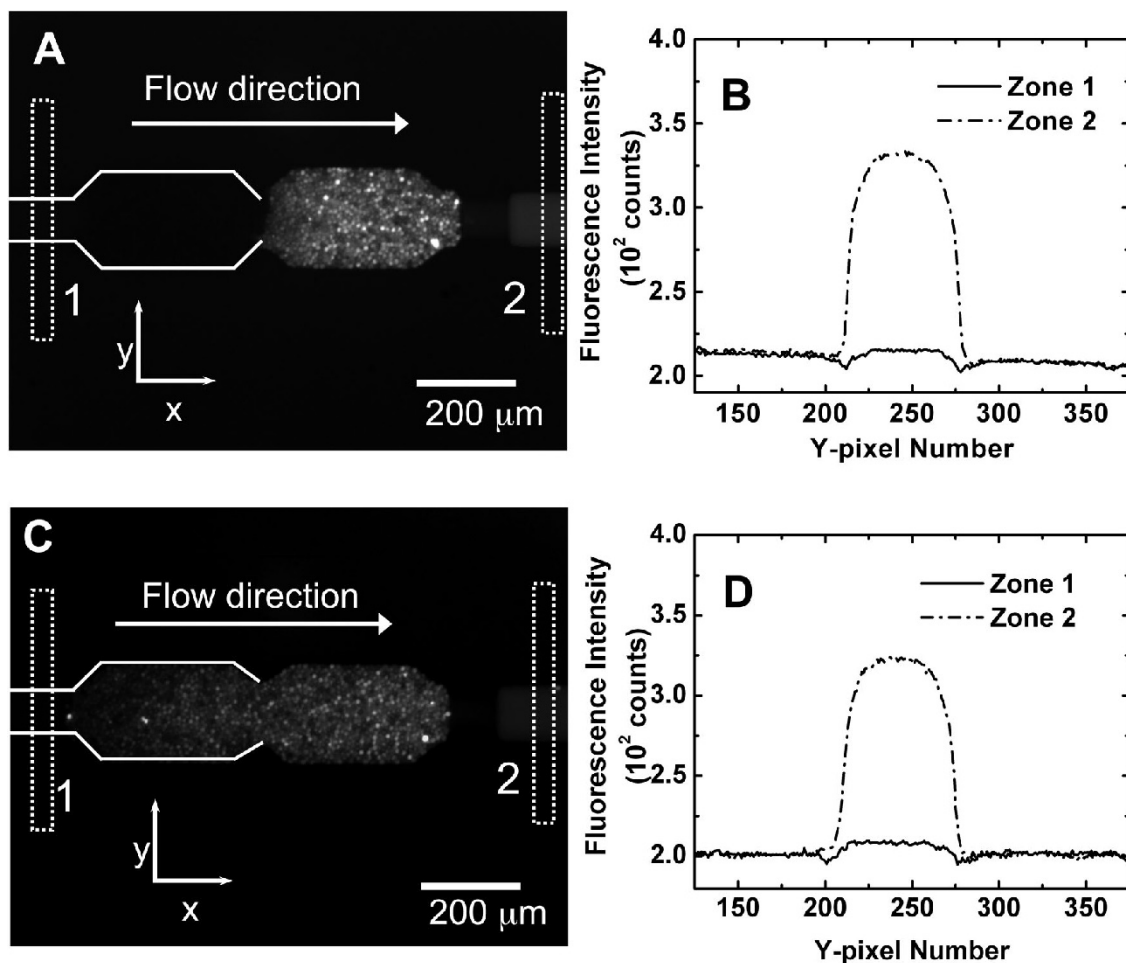
Fig. 3   (A) Fluorescence micrograph of reactor **II** obtained 15 min after a reactant solution consisting of 1.00 mM glucose and 0.80 mM Amplex Red was introduced into the reactor at a flow rate of 0.20 μL/min.   The left and right microchambers were packed with GOx-bearing and HRP-bearing microbeads, respectively. (B) Fluorescence intensity profiles obtained from the zones 1 and 2 indicated by the white dotted box shown in Fig. 3(A). (C) Fluorescence micrograph of reactor **III** obtained with the same condition as that of reactor **II**.   GOx-bearing beads and HRP-bearing beads were mixed in a one-to-one volume ratio off-chip and packed into the two chambers. (D) Fluorescence intensity profiles obtained from zones 1 and 2 indicated by the white dotted box shown in Fig. 3(C). The x and y pixel dimensions are 2 μm, respectively.
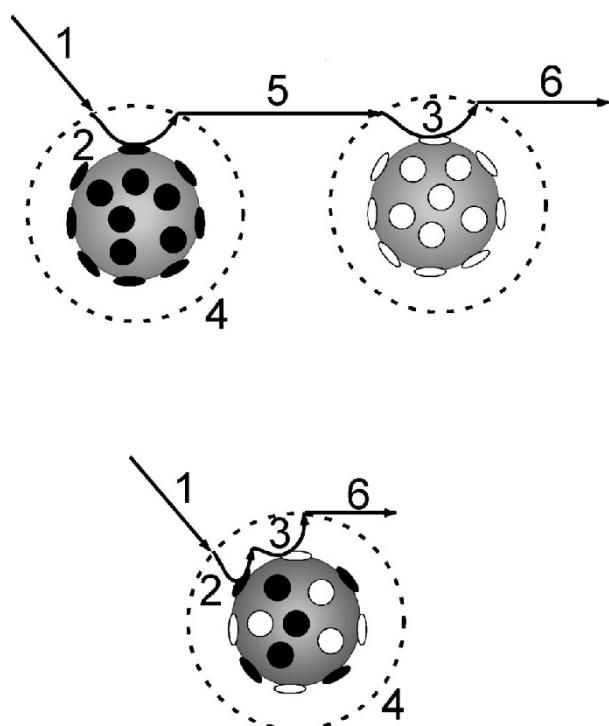
of reactants and products and the kinetics of immobilized enzymes reach a steady state.   The time necessary to reach the steady state is a complicated function of the flow rate, mass-transfer effects of the reactant, intermediate product, and final product, and the kinetics of immobilized enzymes.

The concentrations of the fluorescent product generated from each of the microreactors were quantified using the calibration curve constructed from resorufin standard solutions (Fig. S4, Supporting Information).   The average and the standard deviation of the product concentrations obtained from three-independently prepared devices were 115 ± 4 μM.

In a similar way as above, reactors **II** and **III** (Scheme 1) were examined.   Figures 3A and 3C are fluorescence micrographs of reactors **II** and **III** obtained under the same experimental conditions as that of reactor **I**.   Figures 3B and 3D show the fluorescence intensity profiles obtained from zones 1 and 2 in Figs. 3A and 3C, respectively.   In the case of reactor **II** fluorescence emission was not observed in the first chamber of the sequential reactor, because the beads bearing enzymes for the second step of the sequential enzyme reactions were present

only in the second chamber.   On the contrary, reactor **III** emitted fluorescence in both of the chambers, as shown in Fig. 3C, because the two different sets of beads bearing each of the GOx and HRP enzymes were mixed and packed into all chambers. The fluorescence intensities observed from region 2 of reactors **II** and **III** were seven-times weaker than that from region 2 of reactor **I**.   The steady-state product concentrations produced from reactors **II** and **III** were 4.5 ± 0.2 μM ($n = 3$) and 4.8 ± 0.2 μM ($n = 3$), respectively.   The overall reaction efficiency of these two reactors were ~25-times lower than that of reactor **I**. Note that the fluorescence intensity of resorufin shows a non-linear relationship with the resorufin concentration at a certain concentration range (Fig. S4(B), Supporting Information). There was no significant difference in the reaction efficiency between reactors **II** and **III**.

The better overall reaction efficiency of reactor **I** compared with reactors **II** and **III** can be explained as follows.   The first point is the importance of a mass-transport effect of the intermediate during the sequential, two-step reaction.   In reactor **I**, the GOx and HRP enzymes were co-immobilized in close
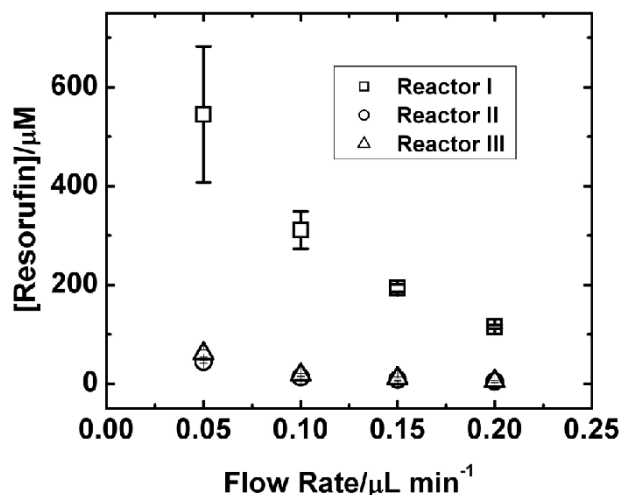
Fig. 4   Plot of the flow rate-dependent concentrations of the resorufin product determined from reactors **I**, **II**, and **III**.   The error bar represents 1σ of three measurements obtained from three independently prepared microfluidic devices.

Scheme 3   Schematic diagrams showing the effect of mass-transport of an intermediate product on the sequential enzyme reactions. The black and white circles indicate GOx and HRP enzymes, respectively. 1. mass-transport of a reactant, 2. GOx-catalyzed reaction, 3. HRP-catalyzed reaction, 4. diffusion layer, 5. mass-transport of an intermediate product, 6. mass-transport of a final product.

proximity to each other on the bead surfaces, and therefore the intermediate product, which was used as a substrate for the second enzyme reaction, could be efficiently converted to a final product without any significant diffusional loss of the intermediate product, as illustrated in Scheme 3.   Digital simulation results confirmed the experimental results.[29]   While an intermediate product was almost non-existent in reactor **I** with the introduction of 1 mM reactant at a flow rate of 0.2 μL/min, ~160 μM of product was estimated to be produced from reactor **I**.   This indicates a fast conversion of the intermediate product to the final product in reactor **I** without significant diffusional loss of the intermediate product. On the other hand, the simulation results of both reactors **II** and **III** showed that ~150 μM of the intermediate product along with ~10 μM of the product was generated from both reactors under the same simulation condition as reactor **I**, suggesting a notable diffusional depletion of the intermediate product in both reactors **II** and **III**.   A similar phenomenon is observed in nature.[23,24] Cells employ intracellular metabolic pathways based on multi-step enzyme reactions.   To increase the overall reaction efficiency, a spatiotemporal control of the intermediate product is essential.[30] A cellular system optimizes the compartmentalization of metabolic pathways to reduce any significant loss of an intermediate product.

Secondly, reactor **I** was less likely to undergo inhibition of GOx enzyme sites by H_2O_2, an intermediate product generated from the GOx-catalyzed reaction of glucose.[31] It was reported that the stability of the GOx enzyme could be greatly improved by adding catalase enzymes to remove H_2O_2 quickly.[32] Thus,

there is less chance of inhibiting GOx enzymes by the intermediate product in reactor **I** than in the other two types of reactors, because the intermediate product can be quickly converted to the final product by having HRP enzymes nearby GOx in reactor **I**.   After rinsing the three microreactors with a buffer solution extensively, we examined whether they can be reused.   The products were produced only 10 – 50% as much as those generated in the first-time use of the reactors, which suggests that they cannot be reused.

Next, we examined the flow-rate effect on the reactor efficiency.   Here, the reactor efficiency was defined as the ratio of the product concentration to the reactant concentration at a given flow rate, and expressed as %.   The final product concentrations were plotted as a function of the flow rate, as shown in Fig. 4.   In general, the product concentration was inversely proportional to the flow rate regardless of the reactor configurations.   When the flow rate decreases, the residence time of substrates in a beads-packed reactor can be prolonged, thus making more contact time between the substrate molecules and the enzymes.   The data also indicates that the two-step enzyme reactions occurring on the beads are not mass-transfer limited.   The overall reaction efficiency of reactor **I** could reach ~50% when the flow rate was reduced to 0.05 μL/min.   On the contrary, the reaction efficiencies of reactors **II** and **III** were <10% at a flow rate of 0.05 μL/min.   This indicates that reactor **I** shows much better efficiency than the other two reactors irrespective of the flow rate.

Conclusions

In summary, we showed that the microfluidic reactor could be an essential platform for examining the overall reaction efficiency of multi-step, sequential enzyme reactions.   The configuration of a microfluidic reactor could be easily modified using simple microfabrication technology and microbeads as a supporting matrix for immobilizing enzymes.   Furthermore, a microfluidic reactor based on immobilized enzymes can be used to mimic the cellular metabolic pathways that employ sequential reactions catalyzed by multiple enzymes, because different

enzymes required for the sequential reactions can be easily localized in designated places in a microfluidic reactor. This platform will be useful to devise new synthetic pathways *in vivo* and screen engineered enzyme pairs for better conversion efficiency. Finally, it is also necessary to develop a theoretical model for quantitatively describing the kinetics of two-step enzyme reactions in a microfluidic reactor. This theoretical work of ours will be reported soon.[29]

Acknowledgements

Supporting Information

Procedures for microfabrication, immobilizing enzymes on microbeads, and determining the binding capacity of avidin-coated beads for biotin–GOx and biotin–HRP along with Figs. S1 – S4 were included in the Supporting Information. This material is available free of charge on the Web at http://www.jsac.or.jp/analsci/.

References

1. R. DiCosimo, J. McAuliffe, A. J. Poulose, and G. Bohlmann, *Chem. Soc. Rev.*, **2013**, *42*, 6437.
2. Y. Asanomi, H. Yamaguchi, M. Miyazaki, and H. Maeda, *Molecules*, **2011**, *16*, 6041.
3. J. Krenkova and F. Foret, *Electrophoresis*, **2004**, *25*, 3550.
4. H. Zhou, Z. Ning, F. Wang, D. Seebun, and D. Figeys, *FEBS J.*, **2011**, *278*, 3796.
5. Q. Zhang, X. Tang, F. Hou, J. Yang, Z. Xie, and Z. Cheng, *Anal. Biochem.*, **2013**, *441*, 51.
6. C. Berne, L. Betancor, H. R. Luckarift, and J. C. Spain, *Biomacromolecules*, **2006**, *7*, 2631.
7. P. Lin, S. Zhao, X. Lu, F. Ye, and H. Wang, *J. Sep. Sci.*, **2013**, *36*, 2538.
8. Y. Gao, R. Zhong, J. Qin, and B. Lin, *Chem. Lett.*, **2009**, *38*, 262.
9. T. Honda, M. Miyazaki, Y. Yamaguchi, H. Nakamura, and H. Maeda, *Lab Chip*, **2007**, *7*, 366.
10. S. Kundu, A. S. Bhangale, W. E. Wallace, K. M. Flynn, C. M. Guttman, R. A. Gross, and K. L. Beers, *J. Am. Chem. Soc.*, **2011**, *133*, 6006.
11. S. Matosevic, G. J. Lye, and F. Baganz, *J. Biotechnol.*, **2011**, *155*, 320.
12. M. S. Thomsen, P. Poelt, and B. Nidetzky, *Chem. Commun. (Cambridge, U. K.)*, **2007**, 2527.
13. P. He, G. Greenway, and S. J. Haswell, *Microfluid. Nanofluid.*, **2010**, *8*, 565.
14. M. B. Kerby, R. S. Legge, and A. Tripathi, *Anal. Chem.*, **2006**, *78*, 8273.
15. G. H. Seong, J. Heo, and R. M. Crooks, *Anal. Chem.*, **2003**, *75*, 3161.
16. A. Guiseppi-Elie, N. F. Sheppard, S. Brahim, and D. Narinesingh, *Biotechnol. Bioeng.*, **2001**, *75*, 475.
17. C. N. Monty, I. Oh, and R. I. Masel, *IEEE Sens. J.*, **2008**, *8*, 580.
18. J. Heo and R. M. Crooks, *Anal. Chem.*, **2005**, *77*, 6843.
19. M. A. Holden, S. Y. Jung, and P. S. Cremer, *Anal. Chem.*, **2004**, *76*, 1838.
20. M.-Y. Lee, A. Srinivasan, B. Ku, and J. S. Dordick, *Biotechnol. Bioeng.*, **2003**, *83*, 20.
21. H. Mao, T. Yang, and P. S. Cremer, *Anal. Chem.*, **2002**, *74*, 379.
22. G. H. Seong and R. M. Crooks, *J. Am. Chem. Soc.*, **2002**, *124*, 13360.
23. K. Mosbach and B. Mattiasson, *Acta Chem. Scand.*, **1970**, *24*, 2093.
24. K. Mosbach, *Sci. Am.*, **1971**, *224*, 26.
25. T. Buranda, J. Huang, V. H. Perez-Luna, B. Schreyer, L. A. Sklar, and G. P. Lopez, *Anal. Chem.*, **2002**, *74*, 1149.
26. D. Losic, J. G. Shapter, and J. J. Gooding, *Langmuir*, **2002**, *18*, 5422.
27. C. Leung, C. Xirouchaki, N. Berovic, and R. E. Palmer, *Adv. Mater.*, **2004**, *16*, 223.
28. M. A. Holden, S. Kumar, A. Beskok, and P. S. Cremer, *J. Micromech. Microeng.*, **2003**, *13*, 412.
29. J. Heo, submitted, **2014**.
30. C. M. Agapakis, P. M. Boyle, and P. A. Silver, *Nat. Chem. Biol.*, **2012**, *8*, 527.
31. J. Bao, K. Furumoto, M. Yoshimoto, K. Fukunaga, and K. Nakao, *Biochem. Eng. J.*, **2003**, *13*, 69.
32. M. Yoshimoto, Y. Miyazaki, M. Sato, K. Fukunaga, R. Kuboi, and K. Nakao, *Bioconjugate Chem.*, **2004**, *15*, 1055.